PAPER • OPEN ACCESS

Cryogenic material properties of additive manufactured 316L stainless steel

To cite this article: K-P Weiss *et al* 2022 *IOP Conf. Ser.: Mater. Sci. Eng.* **1241** 012047

View the article online for updates and enhancements.

Cryogenic material properties of additive manufactured 316L stainless steel

K-P Weiss[1], S Hetzler[1], T Kvackaj[2], R Bidulsky[3], M Actis Grande[3] and D Manfredi[4]

[1] Karlsruhe Institute of Technology, Institute for Technical Physics, Hermann von Helmholtz Platz 1, 76344 Eggenstein-Leopoldshafen, Germany

[2] Technical University of Kosice, Faculty of Materials, Metallurgy and Recycling, Department of Plastic Deformation and Simulation Processes, Vysokoskolska 4, 04200, Kosice, Slovakia

[3] Politecnico di Torino, Dept. Applied Science and Technology, Viale T. Michel 5, 15121 Alessandria, Italy

[4] Politecnico di Torino, Dept. Applied Science and Technology, Corso Duca degli Abruzzi 24, 10129 Torino, Italy

E-mail: klaus.weiss@kit.edu

Abstract. Additive manufacturing is recognized as a potential technology to design and create complex geometries as well as a fast track to build prototype components. Different materials are possible to use, depending on the specific requirements of an application. Superconducting applications like magnets or rotating machines are demanding for the structural components. Either high and/or cyclic mechanical loads can be one of the limiting factors in design. In the cryogenic temperature regime austenitic steels are used due to the mechanical performance and the machinability. In this work 316L austenitic steel samples were produced using laser powder bed fusion, also known as Selective Laser Melting (SLM). Followed by different heat treatments to systematically influence to the microstructure evolution. Beside mechanical properties also thermal properties as heat capacity or expansion are investigated. Having the cryogenic application in mind the tests are conducted at room temperature, liquid Nitrogen and liquid Helium temperature. The measured mechanical and thermal properties are compared to industrial cast austenitic steels to qualify the overall performance of the additive manufactured samples.

1. Introduction

While additive printing of polymer or metallic components advances and is already common for some applications the interest to facilitate this technology for cryogenic components is growing [1]. Especially for superconducting magnets as structural former with complex geometries [2] or rotating machines [3] are demanding applications for the structural components. Therefore, thermal and mechanical loads are of high interest. In this work the material of choice is 316L used widely for cryogenic applications, produced by laser powder bed fusion, also known as Selective Laser Melting (SLM).

2. Material and methods

The used powder was obtained commercially (EOS GmbH, Germany) to be close to the chemical composition of bulk material obtained from classical production route like casting and forging (COMTES, Czech). The chemical composition of the powder material was investigated with a Bruker Q4 TASMAN optical emission spectrometer. The results are given in Table 1 together with material coming from classical casting and forging. The composition is in the range of the definition of grade 316L [4]. Further, the powder was examined for example regarding shape, mean size to be used for the SLM process. The powder is of good quality in spherical geometry and a mean diameter of about 32 μm shown in Figure 1.

The fabrication of the specimen were performed using a EOSINT M270, some details of the printing device are summarized in Table 2. The specimen were produced by SLM close to the final geometry to be machined for further experiment.

As the focus is on cryogenic material properties, the aim was to reduce the number of tests to avoid a high effort of costly cryogenic tests. Therefore, it was decided to focus on the z-direction, namely the building direction, as the loading in direction of the layered structure was identified as one of the most crucial. In Figure 2 the printing orientation together with the cylinders for the tensile or fatigue test after removing the not molten powder from the production table are shown.

For the mechanical tests the necessary specimen were machined from cylinders or plates according to the given standards for tensile [5, 6], fatigue [7], fatigue crack growth rate [8], or fracture toughness [9].

All tests were conducted within the cryogenic material test laboratory (CryoMaK) at the Karlsruhe Institute of Technology [10].

Table 1. Chemical composition of powder and cast material in wt.%

316L	C	Si	Mn	Cr	Mo	Ni	P	S	Fe
powder	0.009	0.32	1.68	18.20	2.79	13.98	0.015	<0.005	Bal.
cast & forging	0.068	0.65	2.02	18.32	1.92	14.12	0.009	0.004	Bal.
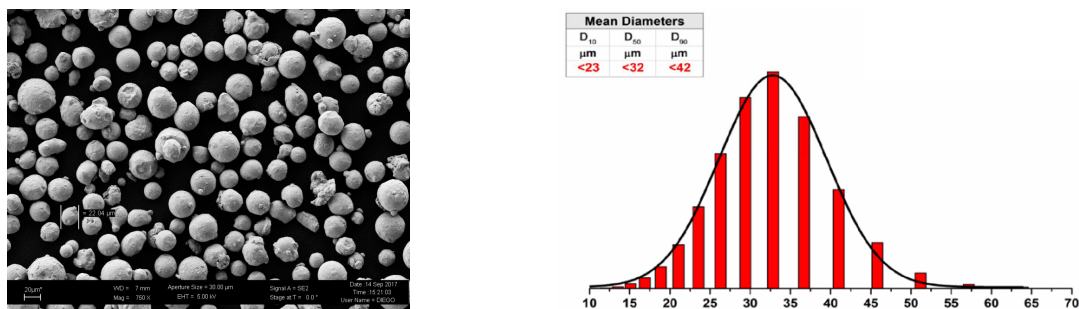
Figure 1. Details of used powder. Left: Electron microscope showing the spherical shape; right: distribution of the diameter.

Table 2. Technical data EOSINT M270 Dual Mode

layer thickness (material-dependent)	20 - 40 μm
laser type	Yb-fibre laser, 200 W
scan speed	50 - 5000 mm/s
laser spot size	100 μm

Figure 2. Details of specimen printing. Left: printing directions, focus on z-direction; mid: cylinders after printing; right: example of fatigue specimen machined from cylinder.

To examine the effect of heat treatment four different states were defined, called HT-0, HT-1, HT-2 and HT-3. The separate HT-4 is for the parallel produced 316L bulk material for comparison to influence the microstructure. In Figure 4 the systematic is depicted:

- The logic is to have first the initial state directly coming from the 3D printing without any heat treatment.
- Second, with HT-1 a moderate stress release treatment at 400°C for 3h is performed.
- Further, a full two stage homogenization heat treatment is done. Stage one at 1050°C for 1h followed by stage two at 700°C for 50h.
- Last, a one-step heat treatment at 1050°C for 1h is done, same as for the bulk material.

The microstructure was investigated after heat treatment. The microstructure looking on the printed layers (first row) as well as the lateral view (second and third row) is given in Figure 5.

For HT0 and HT1 the solidification tracks that are formed according to the laser pattern during printing can still be seen in the top view. Moreover, the melt pool boundaries are clearly visible as seen in the pictures from lateral sections while they are completely erased for HT2 and HT3 due to the high temperature impact during the heat treatment. All specimens show a typical elongation of grains along the building direction which is a typical feature of SLM-specimens.

HT0 and HT1 are more or less comparable. This leads to the conclusion that the moderate stress release heat treatment at 400°C does not have a major impact on this level. However, there is a significant difference looking at HT2 and HT3. After this high temperature heat treatment used in both cases of about 1050°C the typical SLM production patterns are lost. There seems to be no major difference after the single high temperature treatment or the two stage.

Moreover, the material properties itself were investigated for the as-built condition (HT0) in terms of different porosity measurements (Archimedes, image analysis with an optical microscope and computer tomography) and surface roughness measurements. Pores are a reported source for
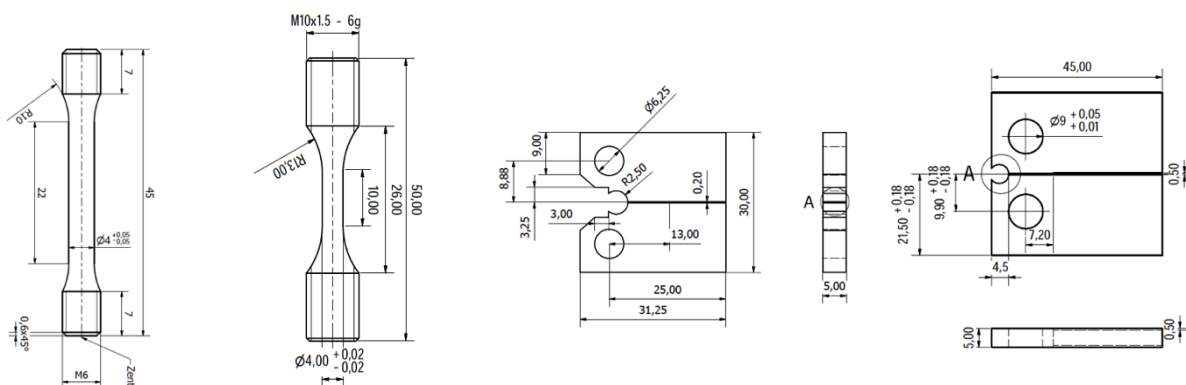
Figure 3. Specimen dimension for tensile, fatigue, fracture toughness, fatigue crack growth rate (from left to right).
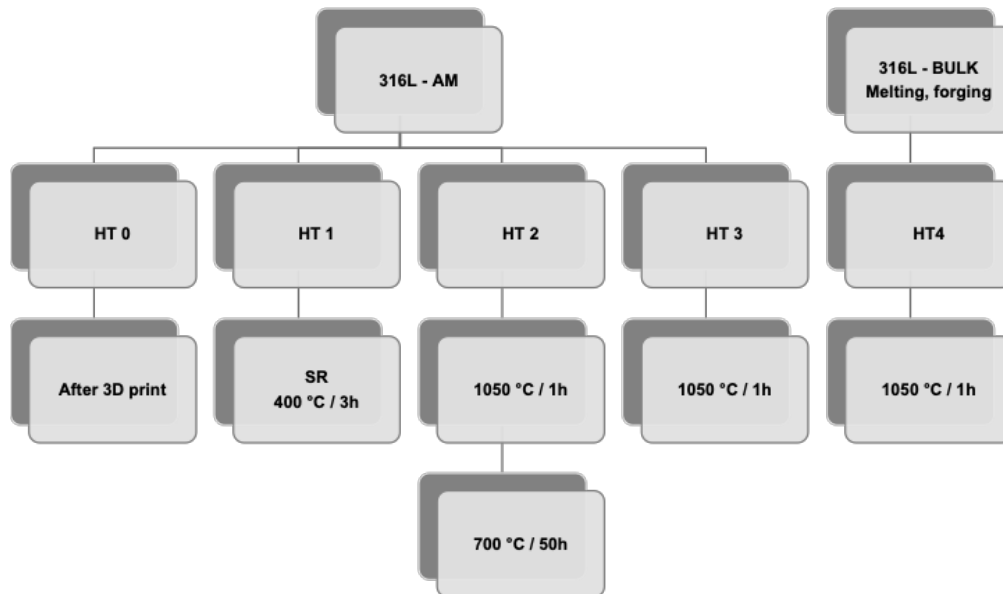
Figure 4. Sspecimen heat treatment systematics for further examination.

premature failure of SLM parts under cyclic loads because they act as localized high stress concentration and crack initiation. Porosity measurements were performed to verify the specification from EOS GmbH (producer of powder and printer) of a porosity below 1%. With a value of 0.5% for the Archimedes measurement and 0.03% for the image analysis, the specification was confirmed.

For the surface roughness measurement, a confocal microscope from NanoFocus was used and the evaluation was executed with a line roughness measurement [11].
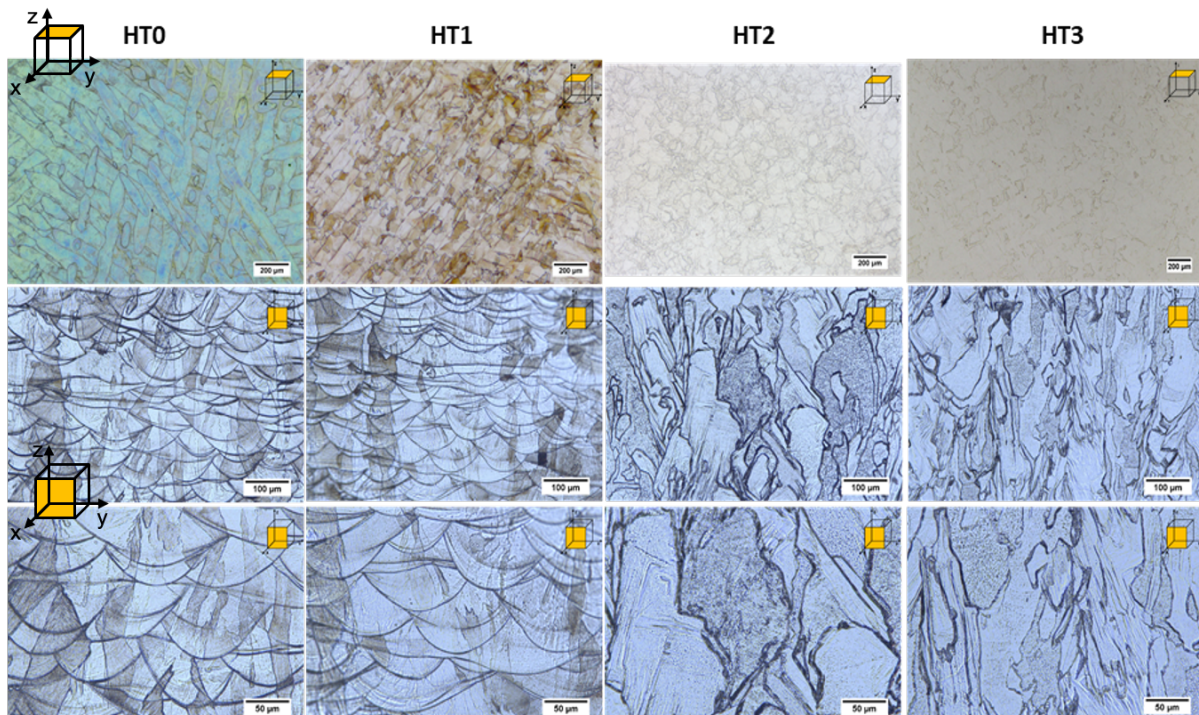
Figure 5. Microstructure overview of HT0, HT1, HT2 and HT3. The observed orientation is indicated by the yellow plane of the inset.
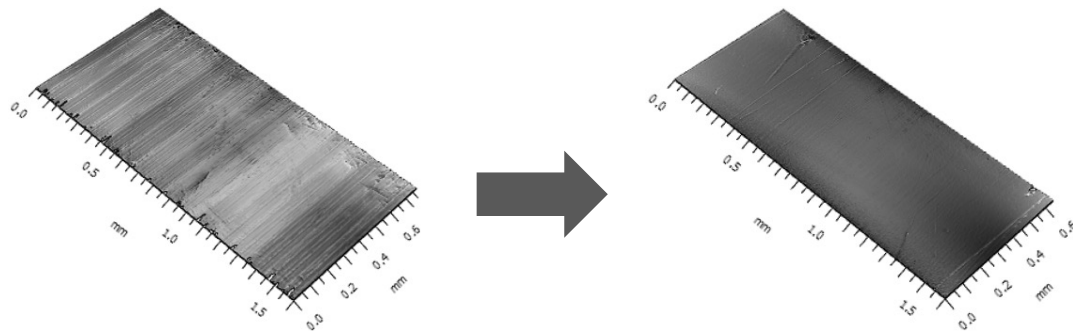
Figure 6. Surface roughness before (left) and after polishing (right).

To avoid premature failure due to surface effects, the specimen were polished to reduce the surface roughness. The roughness was reduced by a factor of approx. ten, reducing the mean maximum peak to valley from $6.5\,\mu$m down to $0.7\,\mu$m. In Figure 6 a control surface of about 1.6 mm x 0.5 mm is shown, depicting the effect of polishing to obtain a smooth surface.

As well as porosity, rough surfaces are often assumed to act as stress raisers and therefore initiate a crack that leads to failure [12]. The surface of the machined specimen had a mean roughness depth of $Rz = 6.53\,\mu$m with a mean standard deviation of $1.3\,\mu$m. By polishing it was possible to decrease the surface roughness to a mean roughness depth of $Rz = 0.7\,\mu$m with a mean standard deviation of $0.4\,\mu$m.

3. Experimental results

3.1. Thermal properties
In Figure 7 the thermal expansion in z-direction as well as the heat capacity of the printed material is shown measured for all different SLM after heat treatment, measured from about 300K down to 4K [10].

As can be seen the heat treatment has no visible impact on the thermal properties. All specimen results collapse on the same measurement curve. Compared to the standard bulk 316L material [13] there seems to be a small difference in the thermal expansion of about 6%. Looking at the heat capacity the curves are almost identical to the bulk specimen.

Altogether the results indicate, that the production process like casting, SLM or heat treatment is not a dominant factor.
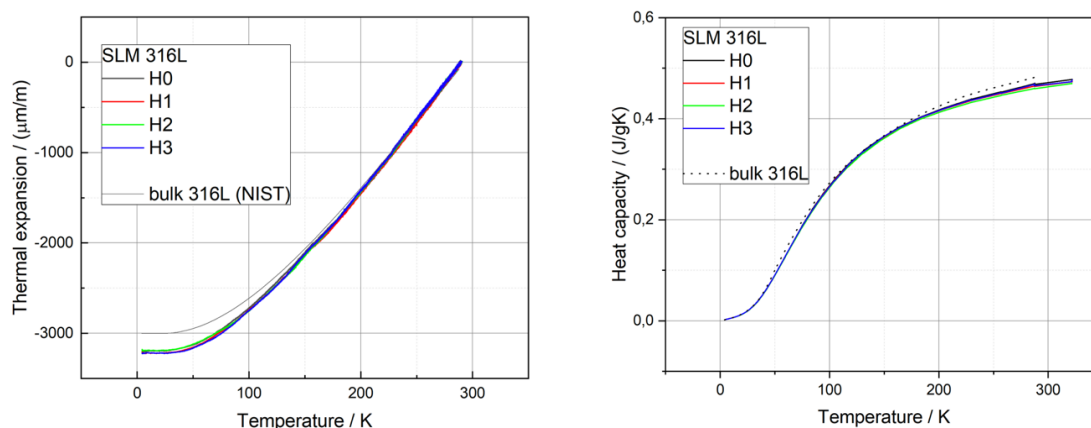
Figure 7. Thermal properties of all SLM material after heat treatment compared to standard 316L for thermal expansion in z-direction (left) and heat capacity (right).

3.2. Tensile tests

Tensile tests have been carried out at ambient 298 K and cryogenic temperature of 77 K and 8 K for all material from HT0 to HT4. The cryogenic test at 77 K was performed in liquid nitrogen. For the 8 K tests an evaporating gas cryostat was used cooled with liquid Helium [10].

The stress-strain curves of all tensile tests are pictured in Figure 3. In addition, a comparison between all heat treatments and traditional manufactured specimens in terms of typical mechanical properties is given in Figure 8. For easier comparison in Figure 9 bar graphs of yield strength, ultimate tensile strength and total elongation are shown.

Looking at the properties of the SLM-built specimens at room temperature, a big decrease in yield strength between HT0, HT1 and HT2, HT3 can be seen. However, HT2 and HT3 exhibit higher strain hardening resulting in a similar ultimate tensile strength than HT0 and HT1. The reason for the poor strain hardening of HT0 and HT1 is still under investigation. Reports from [3], [14], [15] show a similar behavior. Moreover, HT2 and HT3 exhibit a tremendous increase in uniform elongation that is even bigger than for the traditionally manufactured material.

For HT0 and HT1 the mechanical behavior changes significantly at 77 K. Both heat treatments now exhibit strain hardening and the uniform elongation is also in the range of HT2 and HT3 as well as of the traditionally manufactured material.

In summary the mechanical properties of HT2 and HT3 are in the same range as the traditional manufactured material making the SLM-process with an adequate post heat treatment a considerable option for applications under static loads. Disregarding the ductility at room temperature and 8 K, even the yield and ultimate tensile strength of the specimens with no post heat treatment (HT0) are in a similar range to the traditional manufactured material. The typical serrations developing below 40 K are present for all cases.

A detailed discussion of the tensile test results and the microstructure was given in [16].
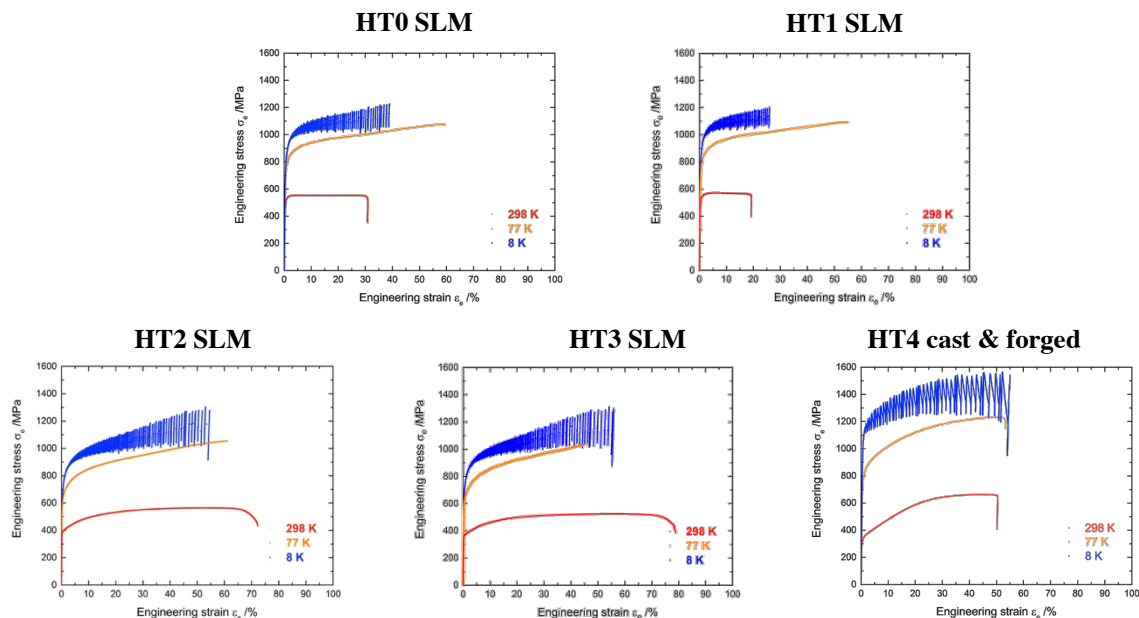
Figure 8. Stress strain curves for all materials HT0 to HT4 measured at room temperature, 77 K and 8 K.
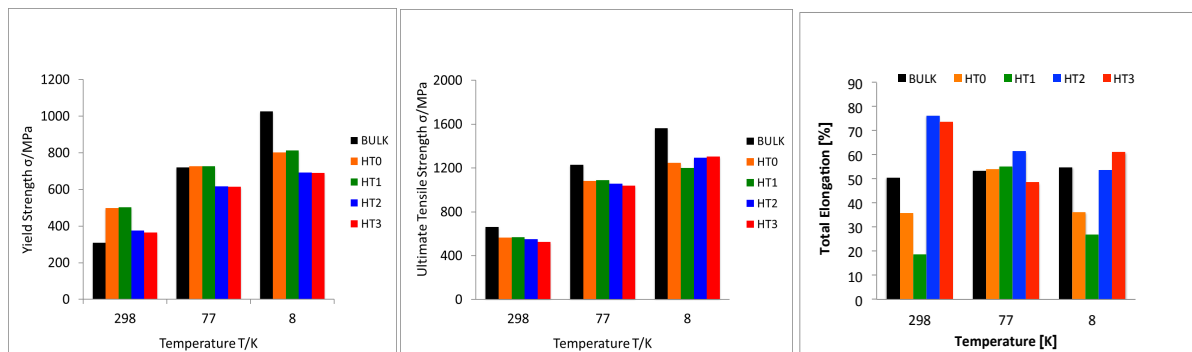
Figure 9. Comparison of yield strength, ultimate tensile strength and total elongation for all specimen.

3.3. Fracture toughness

Further mechanical assessment is done by fracture toughness measurements. Using the J-integral to obtain J_q according to [9] K_{IC} was calculated. To relate the results to the tensile tests the relation between yield strength and fracture toughness K_{IC} is shown in Figure 10 together with the fracture surface of the specimen after test. They show no peculiarities in their appearance. At room temperature high ductility is visible at lower temperatures the typical crack tunnelling is present.

In general, the fracture toughness drops with the test temperature. Having about 300 MPa m^0.5 for the RT tests, between 200 to 240 MPa m^0.5 at 77 K and at 8 K the minimum value is about 160 MPa m^0.5. The results are in line with bulk material measurements [17] considering the error bar.

3.4. Fatigue crack growth rate

Going from quasi static to dynamic behavior under alternating load the fatigue crack growth rate was measured at room temperature and cryogenic temperature at 8 K was measured. The tests were performed under a load ration of 0.1 with constant load. With advancing crack, the differential stress intensity ΔK increased. In Figure 11 the results of all materials are summarized.

The overall crack advance of the SLM specimen da/dn is slightly steeper than the bulk material [17]. However, the slope for all SLM specimen HT0 to HT3 is more or less the same.

Remarkably, at room temperature for the material having the high temperature heat treatment and low yield stress HT2 and the stress release HT3 the critical ΔK_C is reached earlier while the threshold ΔK_{th} seems to be the same for all SLM specimen.

Altogether, it can be concluded that the effect of the SLM production results in a more sensitive fatigue crack growth behavior regardless of heat treatment.
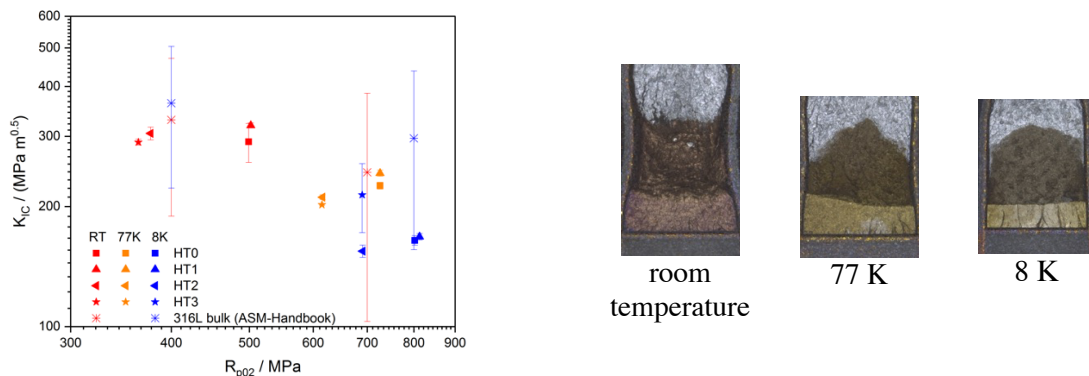
Figure 10. Fracture toughness results versus yield strength for all materials SLM and bulk [17] measured (left). On the right typical crack surface after specimen opening at room temperature, 77 K, and 8 K.
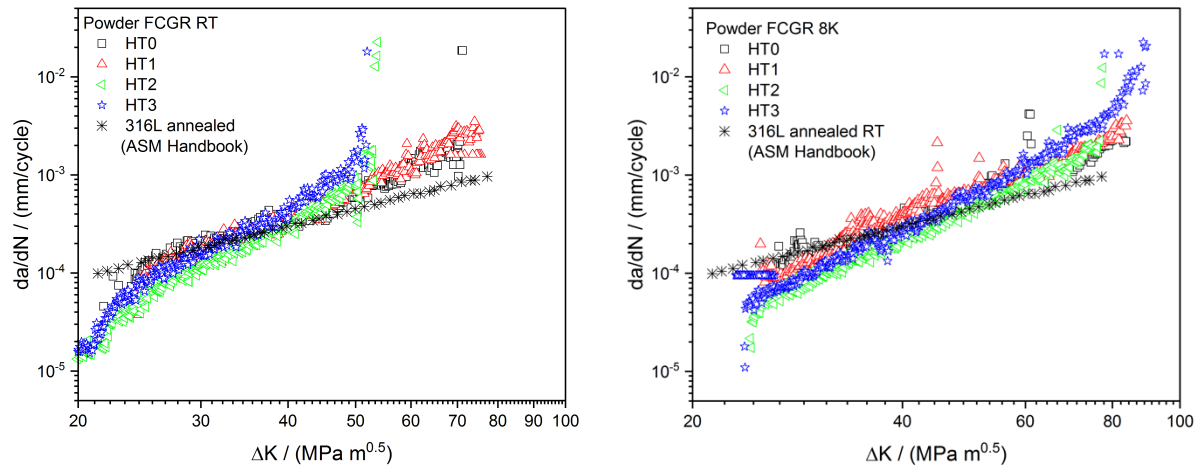
Figure 11. Fatigue crack growth rate measured at room temperature (left) and at 8 K (right) for all materials SLM and bulk material [17].

3.5. High cycle fatigue test

Fatigue tests were also performed for all heat treatments. Specimens were loaded with sinusoidal stresses at frequencies between 20 and 30 Hz and a load ratio of $R = 0.1$ and the reached number of cycles N_f at each maximum stress level are given in Figure 12.

At the top left the high cycle tests at room temperature for the SLM HT0 directly from 3D printing is seen. The maximum stress level was chosen incrementally considering yield and ultimate tensile strength from the tensile tests. However, decreasing the maximum stress level below the yield strength no clear evidence of a fatigue life limit could be deduced. All specimen failed. On the contrary, for given maximum stress levels premature failure of specimen occurred. Especially at 420 MPa one specimen reached a cycling number well above 10 million cycles, while another specimen at the same condition failed already shortly after 300 thousand cycles.

The results of the fatigue tests obtained for HT0 at 77 K exhibit more or less the same arbitrary failure behavior. Especially at about 760 to 770 MPa maximum stress level, there were six specimen tested. Remarkably two of them survived 1 million cycles while one specimen failed before 400 thousand cycles and three below 100 thousand cycles. However, for the 77 K test further specimen tested at 760 MPa and below point to a fatigue limit of about 760 MPa.

The described behavior is visible for all measured SLM specimen from HT0 to HT3. Especially for HT2 at 77 K four specimen tested at the same maximum stress level resulted in a surviving specimen but also three premature failures between 100 thousand and 700 thousand cycles.

The calculated uncertainty does not explain this big scatter of results. This points to the conclusion that for the SLM produced specimen the stress level is not the dominating parameter and the fracture surfaces were investigated.

Tests at 8 K were not performed due to the high amount of specimen needed to perform the RT and 77K fatigue tests and, without clarification of the seen effect at RT and 77 K it was decided to avoid the costly 8 K tests at this stage.

3.6. HCF fracture surface analysis

In Figure 13 the crack initiation spots of different specimens are pictured. In picture (a) to (c) two specimens are shown, that were tested at the same maximum stress level. While specimen (a) (HT0-L2) reached about 100 thousand cycles before failure, specimen (b)/(c) (HT0-N2) showing both sides of the fracture surface, only reached 30 thousand cycles. In specimen HT0-L2 the striations that are caused by cyclic loading are visible and the crack initiation seems to be induced due to a surface scratch or roughness. In comparison to that, specimen HT0-N2 (b)/(c) shows a macroscopic defect that causes the early failure.
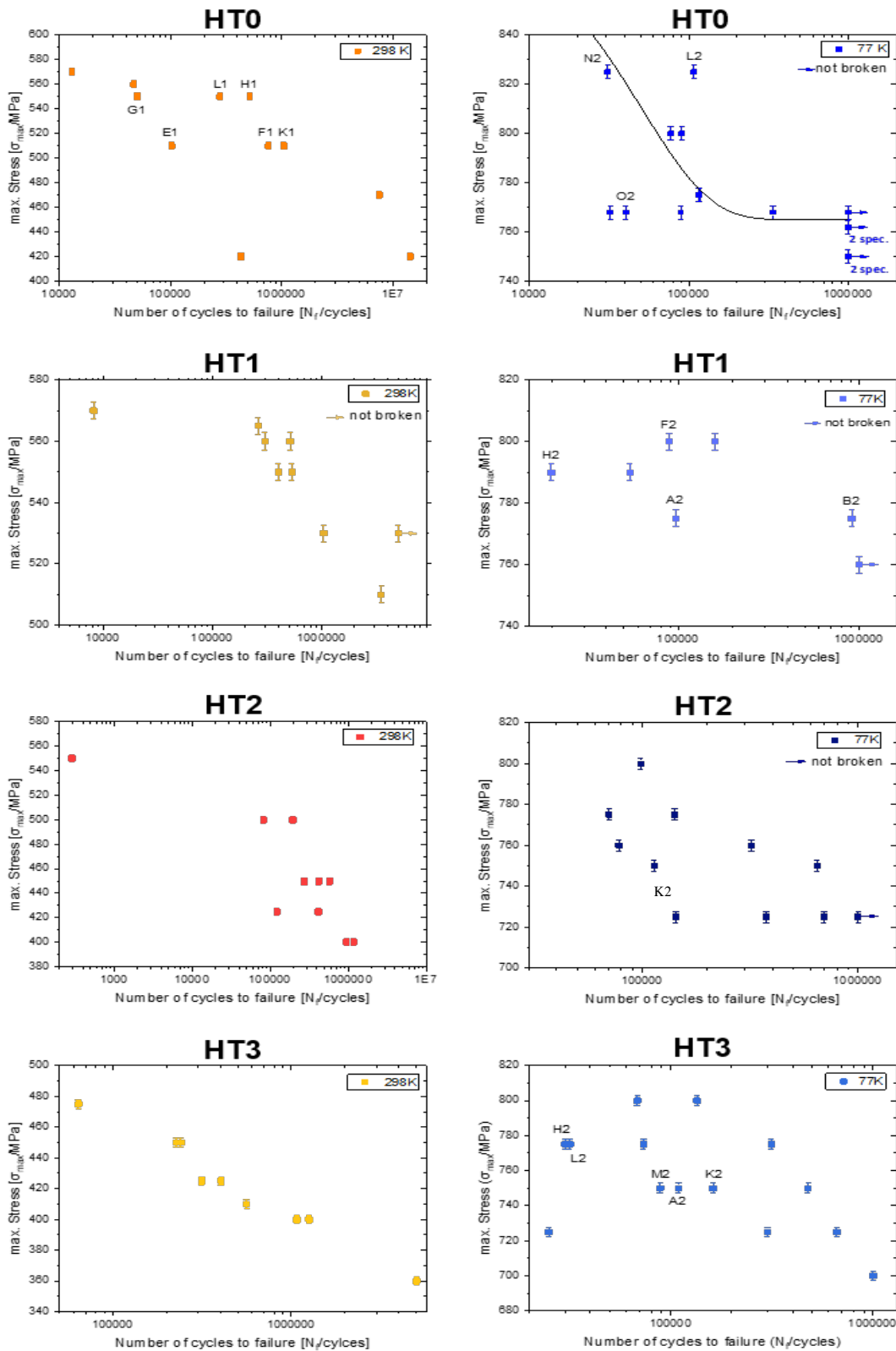
Figure 12. High cycle S-N_f results for all materials HT0, HT1, HT2 and HT3 measured at room temperature (left) and 77 K (right). Named datapoints indicate specimen used for fracture surface investigation.
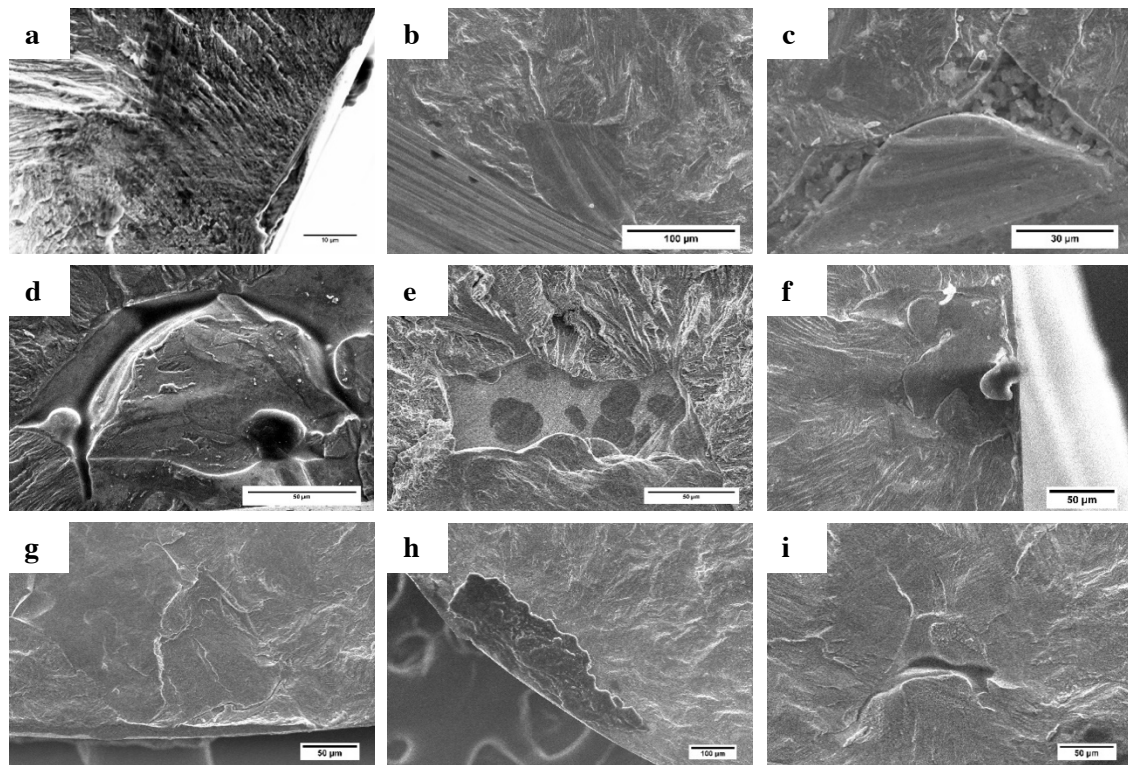
Figure 13. Fracture surfaces of regular (a) and premature failure (b-i). (a) HT0-L2, (b) HT0-N2a, (c) HT0-N2b, (d) HT0-O2, (e) HT0-G1, (f) HT1-F2, (g) HT1-H2a, (h) HT1-H2b, (i) HT2-K2

In picture (b) and (c) small areas with an untypical smooth surface that exhibit no fatigue striations or similar are visible. As expected, similar structures can be seen for specimen that failed after a rather short number of cycles. Such areas are not only found at the direct crack initiation spots but also throughout other areas of some specimens.

These areas appear to come from a lack of fusion between two layers. This could be caused by a localized too low heat input during the SLM-process. While the current layer of powder was molten melt, presumably the heat input was not sufficient to fuse the underlaying layer of solidified material. Such flaws led to a high stress concentration causing early crack initiation and premature failure.

4. Summary and outlook

Although the benefit of additive manufactured 316L is given, great care has to be taken for application. The results coming from the different heat treatment show that the thermal properties are well in line with bulk material from casting and forging. Mechanical tests like tensile, fracture toughness and fatigue crack growth rate can be understood in the light of heat treatment and the influence of the microstructure.

However, high cycle fatigue tests reveal the sensitivity to the quality of the production process. Insufficient fusion of the powder layers lead in this present work to premature failure. This needs to be considered for application. Further possible steps to improve the quality of the material have to be taken into account, like optimization of the SLM process together with a possible quality control (e.g. by CT-scans or ultrasonic testing) to detect such flaws within the material.

5. References

[1] Stautner W, Vanapalli S, Weiss K-P, Chen R, Amm K, Budesheim E, Ricci J, IOP Conference Series: Materials Science and Engineering Volume 278, Issue 1, (2017) 012134

[2]   Kirby G et al. IEEE TRANS.APPL.SUPERCOND., VOL. 27, NO. 4, JUNE 2017

[3]   Kirchheim A, Zumofen L, Gehrig M "Additive Fertigung mit (316L): Prozess- und
       Characterisierungsergebnisse" (2014)

[4]   Steels A, "Stainless Steel Grade Datasheets," Atlas Steels Tech. Dep., pp. 1–2, 2013.

[5]   ASTM E8/E8M-16 "Standard Test Methods for Tension Testing of Metallic Materials"

[6]   ASTM E1450-16 "Standard Test Method for Tension Testing of Structural Alloys in Liquid
       Helium"

[7]   ASTM E466-15 "Standard Practice for Conducting Force Controlled Constant Amplitude Axial
       Fatigue Tests of Metallic Materials"

[8]   ASTM E647-15e1 "Standard Test Method for Measurement of Fatigue Crack Growth Rates"

[9]   ASTM E1820-20 "Standard Test Method for Measurement of Fracture Toughness"

[10]   Sas J, Weiss K-P, Bagrets N, Acta Metallurgica Slovaca 21 (4) (2015), pp. 330-338

[11]   DIN EN ISO 4287:2010-07 and DIN EN ISO 4288:1998-04 "Geometrical Product
       Specifications (GPS) - Surface texture: Profile method"

[12]   William D G R, Callister D, "Materialwissenschaften und Werkstofftechnik" 8th ed.
       Weinheim: Wiley-VCH Verlag GmbH & Co. KGaA, 2013.

[13]   Cryogenic material properties: https://trc.nist.gov/cryogenics/materials/materialproperties.htm
       (2021)

[14]   Spierings A B, Starr T L, Wegener K, Rapid Prototyp. J., vol. 19, no. 2, pp. 88–94, 2013.

[15]   Lackey A D, "Comparative Study of Mechanical Properties of 316L Stainless Steel Between
       Traditional Production Methods and Selective Laser Melting",Western Carolina
       University. ProQuest Dissertations Publishing, 2016. 10103725

[16]   Bidulskỳ R, Bidulská J, Gobber F S, Kvačkaj T, Petroušek P, Actis-Grande M, Weiss K-P,
       Manfredi D, Materials, 2020, 13(15), 3328

[17]   ASM Handbook, Volume 19, "Fatigue and Fracture", ISBN: 978-0-87170-385-9 (1996)